Supporting Information

Tailoring the electronic structure of In_2O_3/C photocatalysts for enhanced CO_2 reduction

Awu Zhou,[a b] Chen Zhao,[b] Jianchi Zhou,[a] Yibo Dou,*[a] Jian-Rong Li[b] and Min Wei[a]

[a]*State Key Laboratory of Chemical Resource Engineering, Beijing University of Chemical Technology, Beijing 100029, PR China*

[b]*Beijing Key Laboratory for Green Catalysis and Separation and Department of Chemistry and Chemical Engineering, Beijing University of Technology, Beijing 100124, P. R. China*

E-mail: *douyb@buct.edu.cn*

1. Supplemental Experimental Procedures:

1.1 Preparation of hexagonal M-MIL-68 (In) (M = Cu, Zn, and Fe)

MIL-68 (In) was synthesized according to a previously reported solvothermal method.[1, 2] As for MIL-68 (In), $In(NO_3)_3$ (0.6 mmol), and terephthalic acid (1.1 mmol) were dissolved in 80 mL *N,N*-dimethylformamide (DMF). After stirring under ultrasonic concussion for 15 minutes, the mixture was placed in an oil bath at 120 ^oC for 6 hours. Then, the products were collected and washed with deionized water and ethanol and dried under vacuum at 60 °C. Cu-MIL-68 (In) was prepared by a similar procedure of using $Cu(NO_3)_2 \cdot 3H_2O$ (0.075 mmol) and $In(NO_3)_3$ (0.525 mmol) as the metal source. In addition, the Fe-MIL-68 (In) and Zn-MIL-68 (In) were prepared by a similar method, in which $Fe(NO_3)_3 \cdot 9H_2O$ and $Zn(NO_3)_2 \cdot 6H_2O$ were used instead of $Cu(NO_3)_2 \cdot 3H_2O$, respectively.

1.2 Preparation of hexagonal M-In_2O_3/C (In) (M = Cu, Zn, and Fe) nanotube

The photocatalysts (In_2O_3/C, Cu-In_2O_3/C, Zn-In_2O_3/C, and Fe-In_2O_3/C) were derived from MIL-68 (In), Cu-MIL-68 (In), Zn-MIL-68 (In), and Fe-MIL-68 (In) by pyrolysis treatment, respectively. Typically, M-In_2O_3/C was synthesized *via* calcination of the obtained M-MIL-68 (In) at 500 ^oC for 45 min under N_2 with 5 ^oC min^{-1}.

1.3 Preparation of hexagonal M-In_2O_3 (In) (M = Cu, Zn, and Fe) nanotube

The photocatalysts (In_2O_3, Cu-In_2O_3, Zn-In_2O_3, and Fe-In_2O_3) were synthesized *via* calcination of obtained MIL-68 (In), Cu-MIL-68 (In), Zn-MIL-68 (In), and Fe-MIL-68 (In), respectively. Typically, M-In_2O_3 was synthesized *via* calcination of the M-MIL-68 (In) at 500 ^oC for 6 hours under air with 5 ^oC min^{-1}.

1.4. Photoreduction reaction

The photocatalytic CO_2 reduction reaction was performed in a closed stainless reactor (50 mL in capacity) with a quartz window. Typically, 30 mg photocatalyst and 50 μL triethylamine (TEA) were spread in the reactor. The photoreactor system was firstly washed with N_2, and then high purity CO_2 (≥99.999%) bubbled through water

was introduced into the reactor with 0.1 MPa pressure. Under full spectrum irradiation (300 W xenon lamp with an optical density of 2550 mW cm^{-2}), the products formed were detected in a fixed time interval. The carbon species were analyzed using a gas chromatograph (GC, Agilent 7890B) equipped with a thermal conductivity detector (TCD) detector and He served as the carrier gas. The produced H_2 and O_2 were analyzed by GC (Shimadzu GC2014C) equipped with a TCD detector using N_2 as carrier gas. The CO and CH_4 selectivity can be obtained by following the formula that

$$\text{CO selectivity (\%)} = \frac{Yield\ of\ CO}{Yield\ of\ all\ products} \times 100\%$$

$$\text{CH_4 selectivity (\%)} = \frac{Yield\ of\ CH_4}{Yield\ of\ all\ products} \times 100\%.$$

The experiments on apparent quantum efficiency (AQE) of CO were performed under a monochromatic light beam with an excitation wavelength (λ) of 380 nm. The average intensity (I) of irradiation was determined to be 183 mW cm^{-2} by a light meter (PL-MW2000 Photoradiometer, PerfectLight) at room temperature. The irradiation area (S) was controlled to be 14.5 cm^2. The number of incident photons (N) is calculated by equations: $N = \frac{E\lambda}{h\,c}$, where E is the total incident energy on the photocatalyst (J), h is Planck's constant (6.626 × 10^{-34} J s), c is the speed of light (3×10^8 m s^{-1}), N_A is Avogadro's number (6.02×10^{23} mol^{-1}).

After 2 h, the CO amounts ([CO]) of Cu-In_2O_3/C, Zn-In_2O_3/C, and Fe-In_2O_3/C nanotubes are 0.62 μmol, 0.43 μmol, 0.31 μmol, respectively.

Based on equations: $\text{AQE (CO)} = \frac{2 \times \text{the number of evolved CO molecules}}{\text{the number of incident photons}} \times 100\%$, the AQE (CO) of Cu-$In_2O_3$/C, Zn-$In_2O_3$/C and Fe-$In_2O_3$/C at 380 nm is about 2×$10^{-3}$%, 1×$10^{-3}$% and 1×$10^{-3}$%, respectively.

1.5 Photoelectrochemical measurements

The CO_2 photoreduction system is a gas-solid reaction, instead of a solid-liquid

reaction. Therefore, it is difficult to provide similar conditions for PEC or EIS measurements. Alternately, we conducted photoelectrochemical measurements by using 0.5 M Na_2SO_4 as the electrolyte, which is reported as a general measurement condition in photocatalytic CO_2 reduction.[3,4] Photoelectrochemical (PEC) measurements were performed on a CHI 660E electrochemical work station (Chenhua Instrument, Shanghai, China) in a standard three-electrode system with the photocatalyst-coated Fluorine-Tin-Oxide (FTO) as the working electrode, Pt plate as the counter electrode, and Ag/AgCl as the reference electrode. A 0.5 M Na_2SO_4 solution was used as the electrolyte. The as-synthesized sample (1 mg) was added into 50 μL Nafion and 2.0 mL methanol mixed solution, and the working electrode was prepared by dropping the suspension (100 μL) onto the surface of an FTO plate (1×1 cm^2). The working electrode was dried at room temperature, and the photo-responsive signals of the samples were measured under chopped light at 0.5 V. The electrochemical impedance spectroscopy (EIS) was performed on the Zennium electrochemistry work station in a standard three-electrode system. The EIS measurement was performed with a bias potential of −0.6 V with a frequency range from 10^{-2} to 10^5 Hz.

1.6 Characterization

Powder X-ray diffraction (PXRD) patterns were recorded on an XRD-6000 (Rigaku Co.) diffractometer with Cu Kα (λ = 1.5418 Å) radiation (40 kV, 30 mA), with a scan step of 0.02°. Fourier transform infrared (FT-IR) spectra were obtained on a Vector 22 (Bruker) spectrophotometer with 2 cm^{-1} resolution. The *in situ* diffuse reflectance infrared Fourier transform spectroscopy (DRIFTS) measurement was carried out in a quartz cell equipped with KBr windows allowing sample activation and successive measurements. The DRIFTS were recorded with a Nicolet 380 instrument spectrophotometer at a spectral resolution of 4 cm^{-1} and an accumulation of 64 sans. Raman spectra were obtained on a Renishaw instrument (in Via-Reflex, 633 nm). UV-vis absorption spectrum was recorded on a Shimadzu UV-2600 spectrophotometer in the wavelength range of 200−800 nm. Solid-state UV-vis diffuse absorption spectra were recorded on a Shimadzu UV-2600 spectrometer equipped with an integrating

sphere attachment at room temperature and a white standard of $BaSO_4$ was used as a reference. X-ray photoelectron spectroscopy (XPS) was obtained on an ESCALAB 250Xi XPS spectrometer (Thermo Fisher Scientific) using Al Kα radiation. CO_2 adsorption/desorption isotherms at 298 K and N_2 adsorption/desorption isotherms were measured on a Micrometitics Surface Area Analyzer (ASAP 2020). Electron spin resonance spectra were recorded on Bruker ELEXSYS CW-EPR electron paramagnetic resonance spectrometer. The morphology of the samples was investigated using a scanning electron microscope (SEM Zeiss SUPRA 55) with an accelerating voltage of 20 kV, combined with energy dispersive X-ray spectroscopy (EDS) for the elemental analysis. Transmission electron microscopic and high-resolution transmission electron microscopic (TEM and HR-TEM) images were recorded on the JEOL JEM-2100 instrument at an accelerating voltage of 200 kV. Elemental mapping images were recorded with an X-ray energy dispersive spectroscopy (EDX) attached to TEM.

1.7 The calculation of band gap energy

Kubelka-Munk function and Tauc equation were utilized to calculate the band gap of the materials.[5, 6] The Kubelka-Munk function F(R) is as follows:

$$F(R) = \frac{(1-R)^2}{2R} \qquad \text{Equation (S1)}$$

Where R is the absolute reflectance of the sample.

And Tauc equation is as follows:

$$(\alpha h\nu)^{1/n} = A(h\nu - E_g) \qquad \text{Equation (S2)}$$

Where α, h, ν, E_g and A are the absorption coefficient, Planck's constant, frequency of the incident photon, band gap of the materials and constant depending on the properties of the material.

The DRS of the sample is converted to Kubelka-Munk function as F(R) is proportional to the absorption coefficient. The α in the Tauc equation is substituted with F(R). Hence, the converted equation is as follows:

$$[F(R)h\nu]^{1/n} = A(h\nu - E_g) \quad \text{Equation (S3)}$$

which can correspond to a permitted direct (n = 0.5), permitted indirect (n = 2), prohibited direct (n = 1.5), or prohibited indirect transition (n = 3).

The graph on plotting $[F(R)h\nu]^{1/n}$ versus *hν*, the tangent line drawn along the slope of the spectra which intersection point with the x-axis gives an estimate of the band gap energy.

2. Computation section

2.1 Model construction and Computational method

Theoretical exploration was completed with CASTEP module. Plane wave was used to perform the DFT calculation with GGA-PBE level. In_2O_3 and Cu-In_2O_3 were constructed according to the experimental PXRD pattern (Fig. 2A). The space group of In_2O_3 is Cubic $Ia\bar{3}$, with the lattice parameters, $a = b = c = 10.118$ Å, $\alpha = \beta = \gamma = 90°$. The supercell of In_2O_3 is 2 × 2 × 2 in the a-, b-, and c- directions, respectively. The structural model and photocatalytic CO_2 reduction calculation were consistent with our previous work.[7]

3. Supplementary Figures and Table

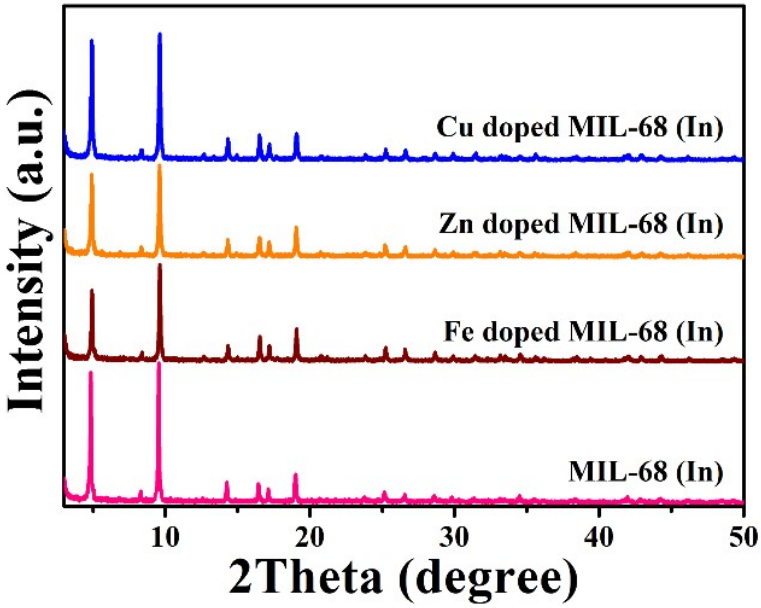

Fig. S1. XRD patterns of MIL-68 (In), Cu-MIL-68 (In), Fe-MIL-68 (In), and Zn-MIL-68 (In).

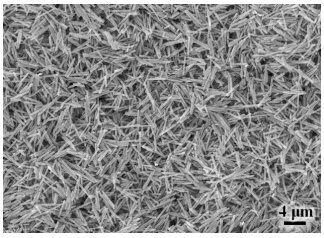

Fig. S2. SEM image of Zn-MIL-68 (In).

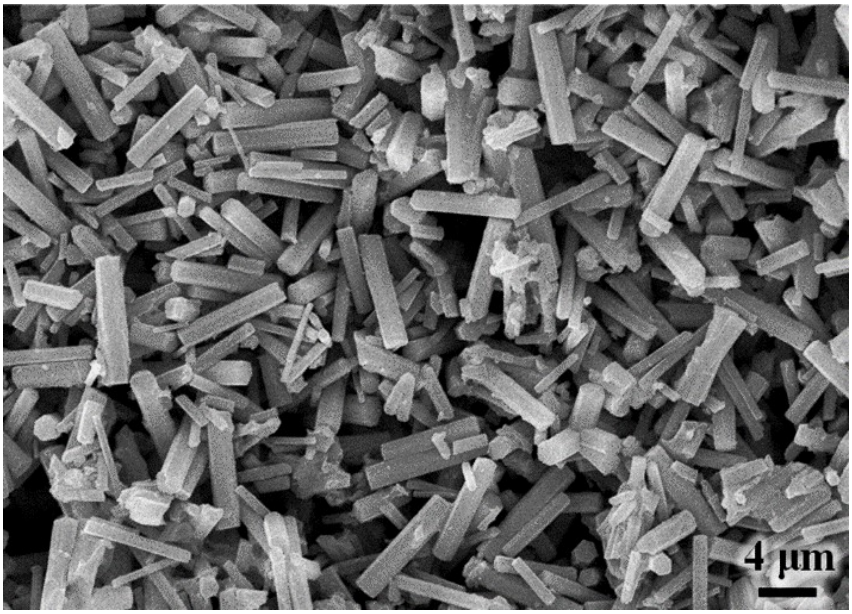

Fig. S3. SEM image of Fe-MIL-68 (In).

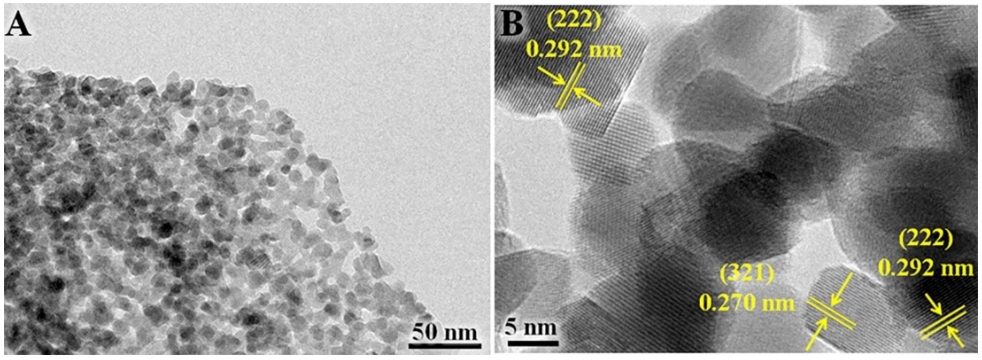

Fig. S4. (A) TEM and (B) HR-TEM images of In_2O_3/C.

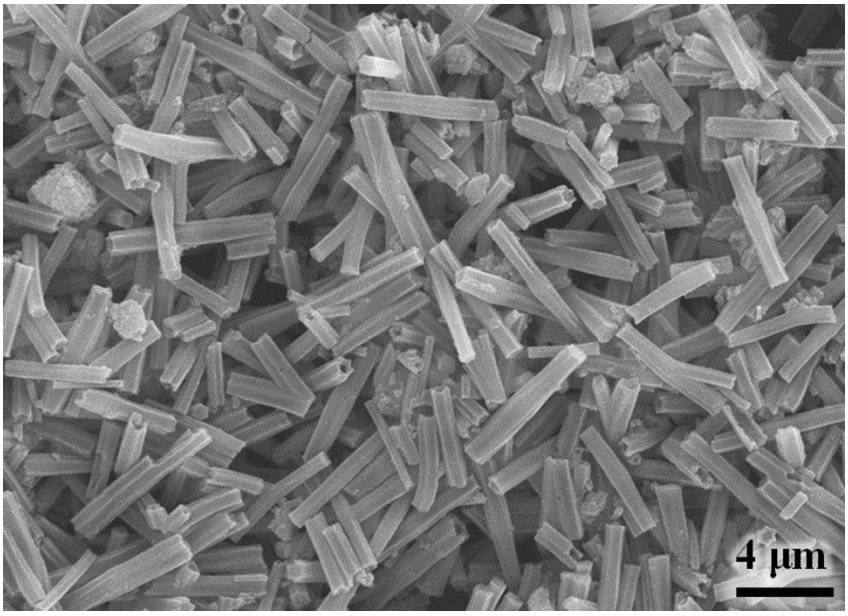

Fig. S5. SEM image of Zn-In_2O_3/C.

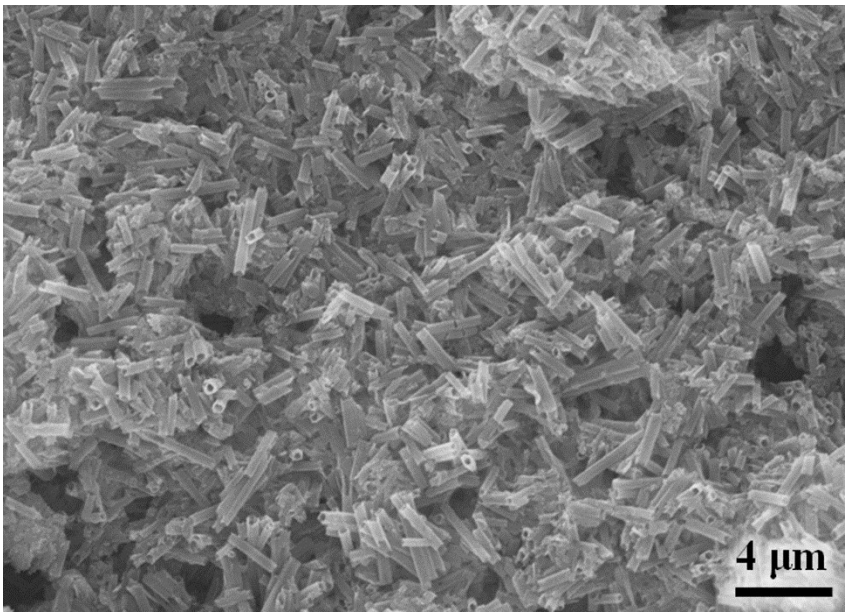

Fig. S6. SEM image of Fe-In_2O_3/C.

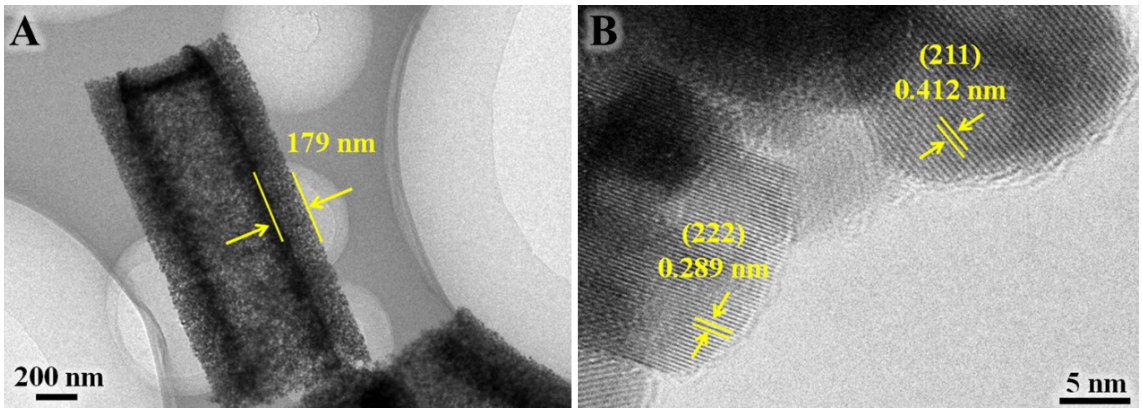

Fig. S7. (A) TEM and (B) HR-TEM images of Zn-In_2O_3/C.

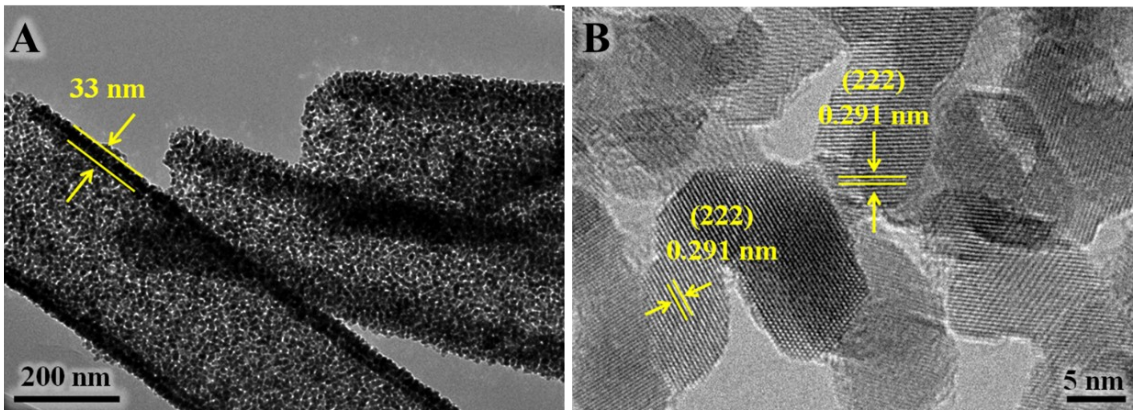

Fig. S8. (A) TEM and (B) HR-TEM images of Fe-In_2O_3/C.

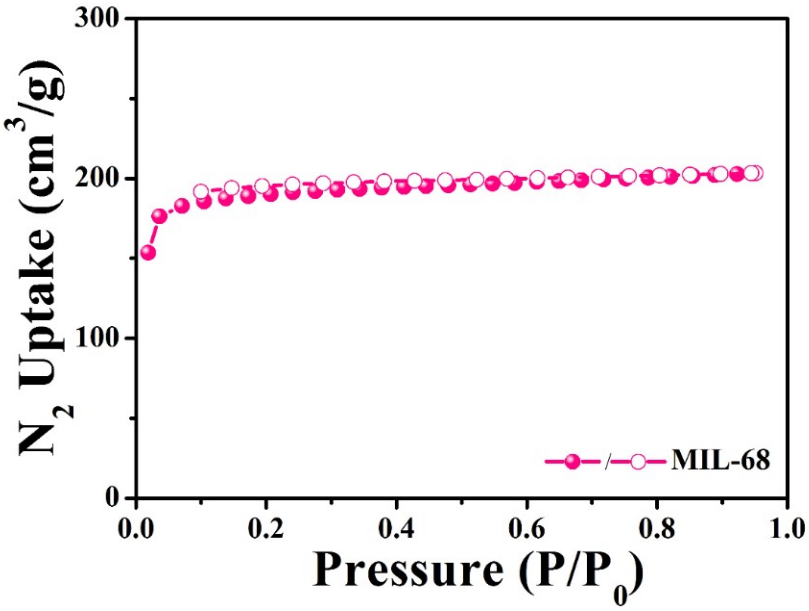

Fig. S9. N_2 adsorption/desorption isotherm of MIL-68 (In).

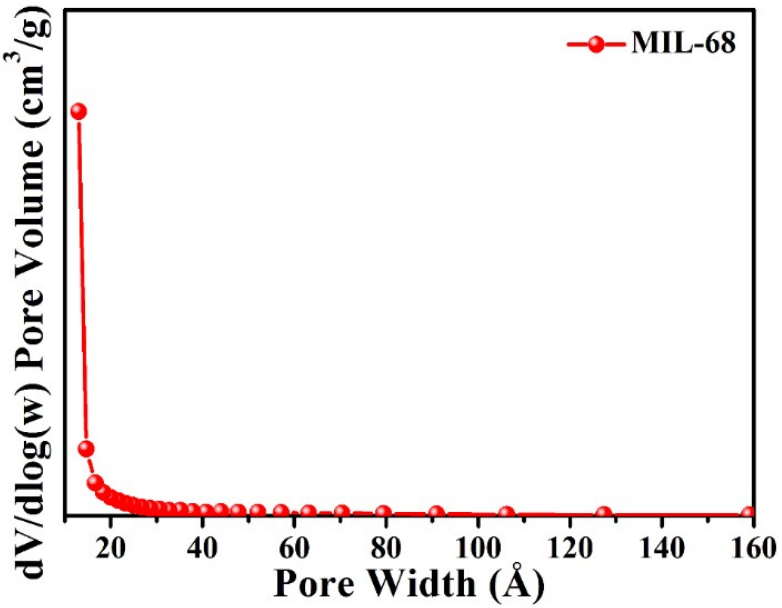

Fig. S10. The pore size distribution of MIL-68 (In).

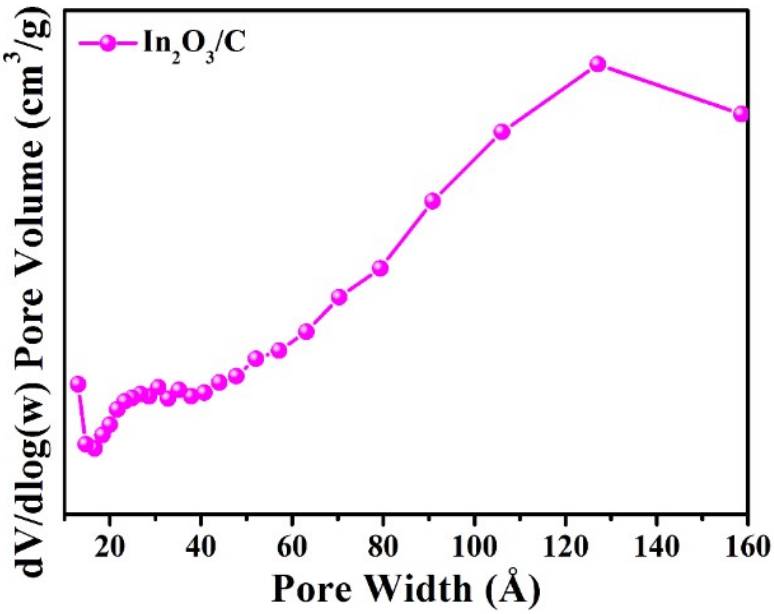

Fig. S11. The pore size distribution of In_2O_3/C.

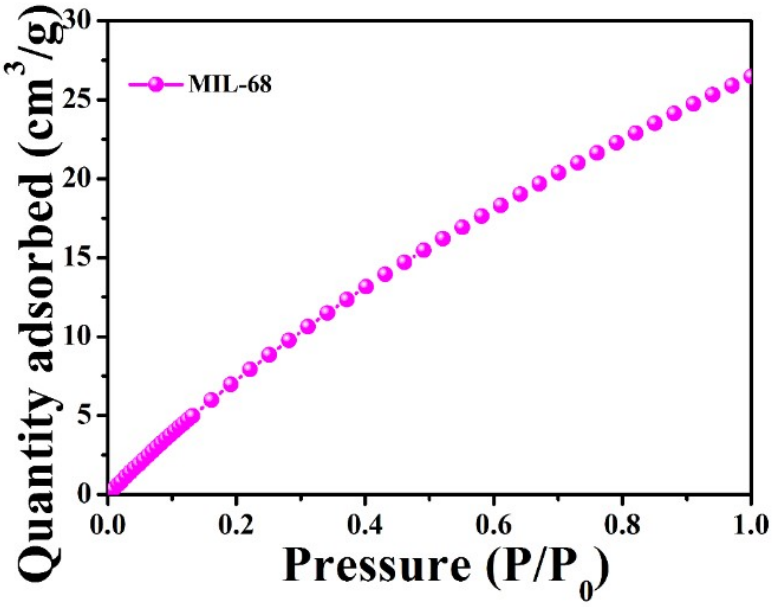

Fig. S12. CO_2 adsorption isotherms of MIL-68 (In).

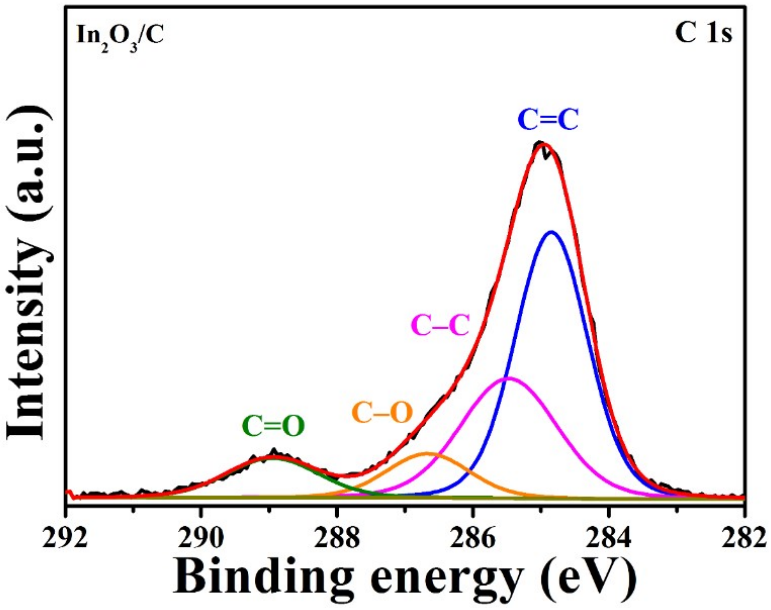

Fig. S13. High-resolution C 1s XPS spectrum for In_2O_3/C.

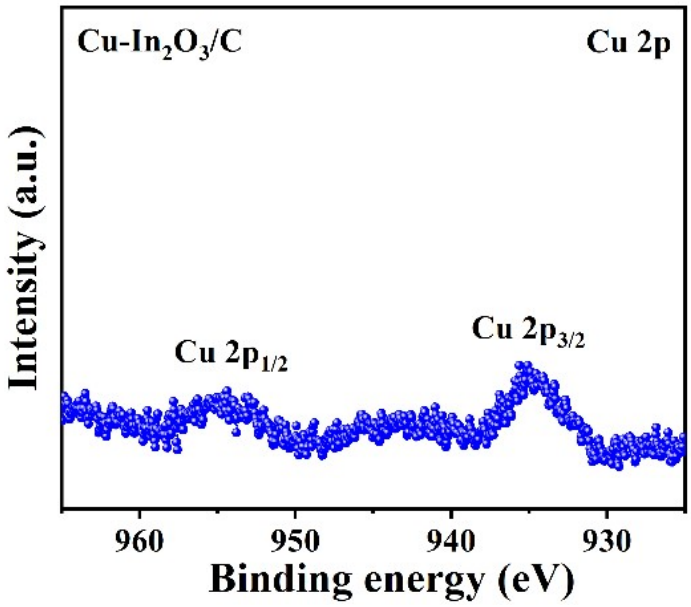

Fig. S14. High-resolution Cu 2p XPS spectra of Cu-In_2O_3/C.

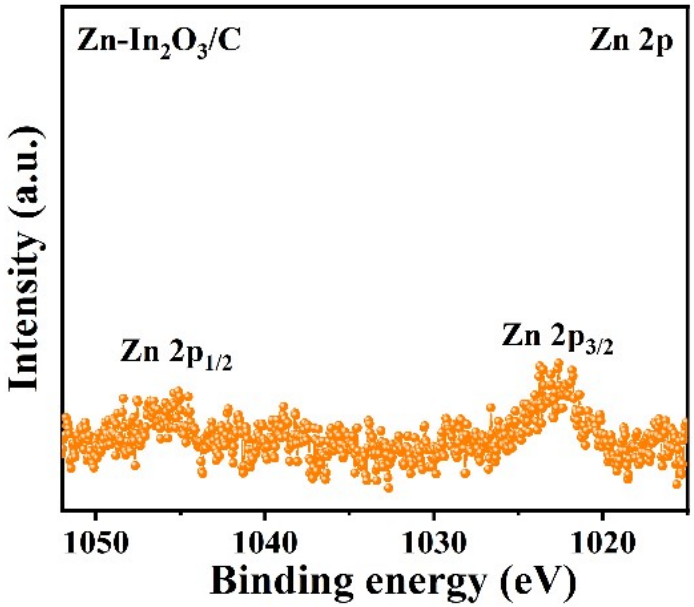

Fig. S15. High-resolution Zn 2p XPS spectra of Zn-In_2O_3/C.

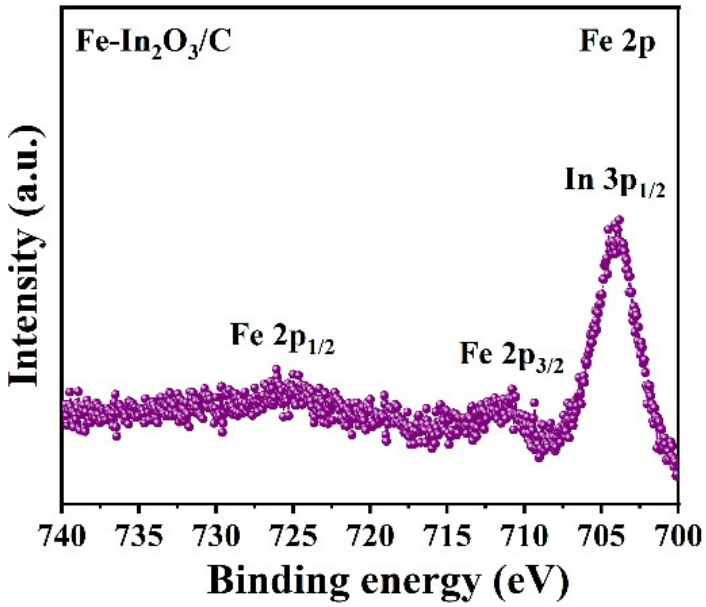

Fig. S16. High-resolution Fe 2p XPS spectra of Fe-In_2O_3/C.

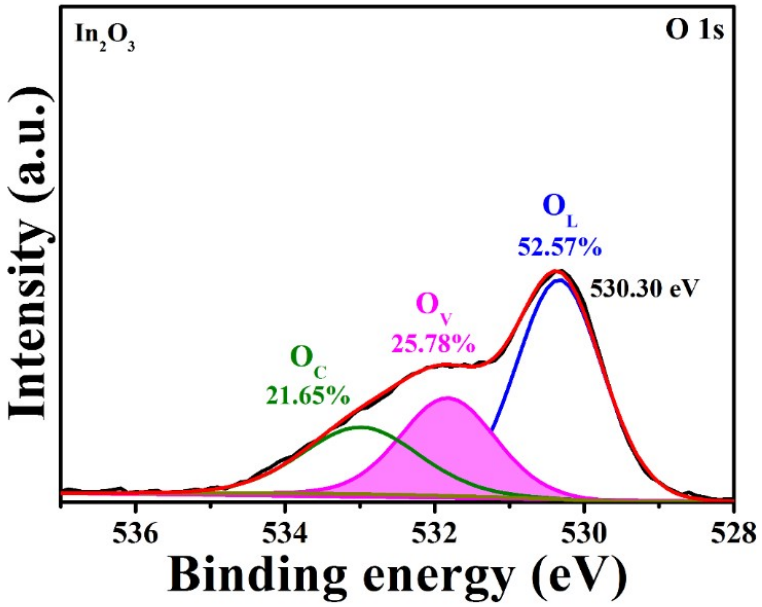

Fig. S17. High-resolution O 1s XPS spectrum for In_2O_3/C.

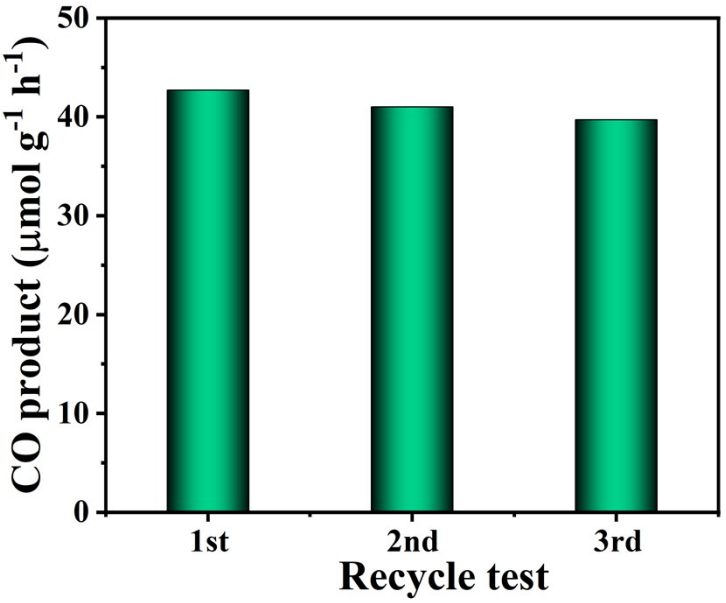

Fig. S18. The recycle experiments of the Cu-In_2O_3/C.

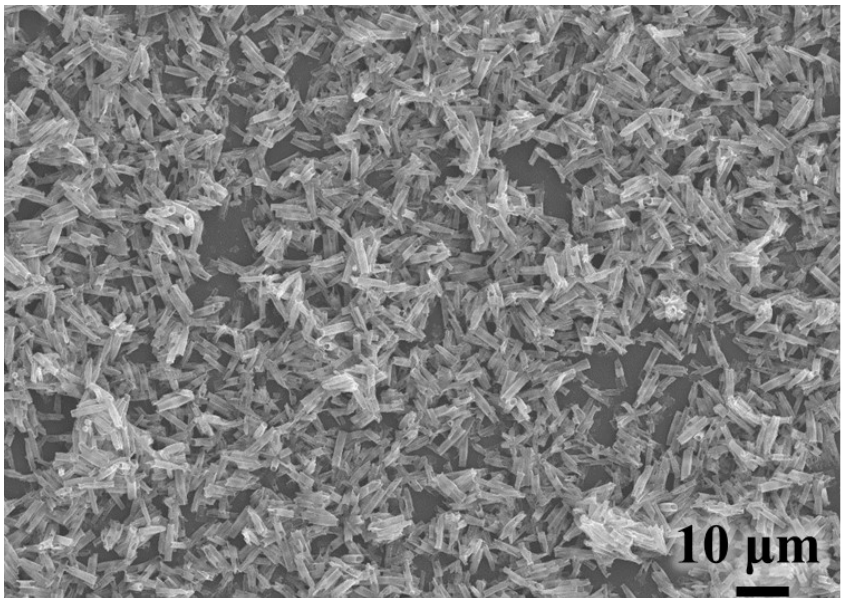

Fig. S19. SEM image of Cu-In_2O_3/C after photocatalytic CO_2 reduction

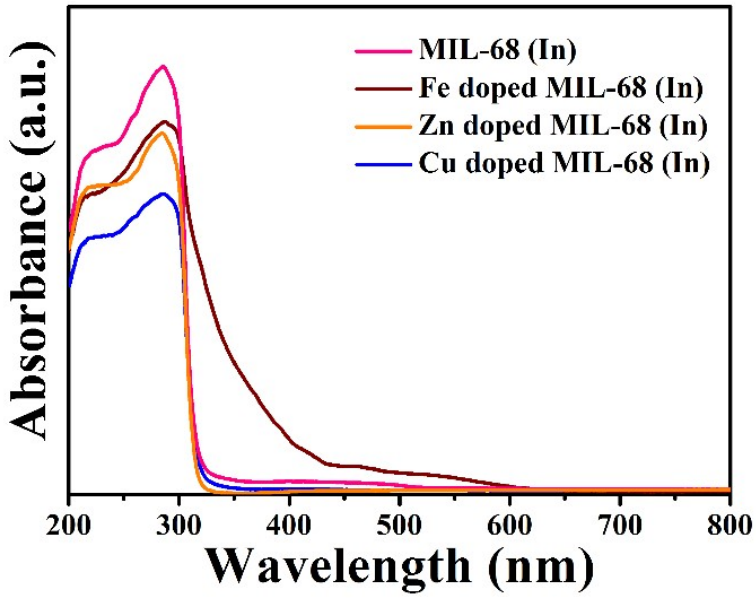

Fig. S20. UV-Vis diffuse reflectance spectra of MIL-68 (In), Zn- MIL-68 (In), Cu-MIL-68 (In), and Fe- MIL-68 (In), respectively.

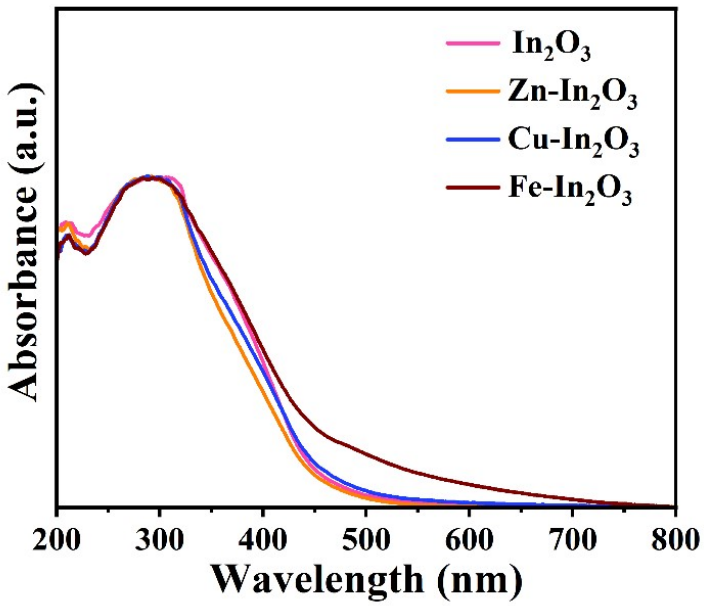

Fig. S21. UV-Vis diffuse reflectance spectra of In_2O_3, Zn-In_2O_3, Cu-In_2O_3, and Fe-In_2O_3, respectively.

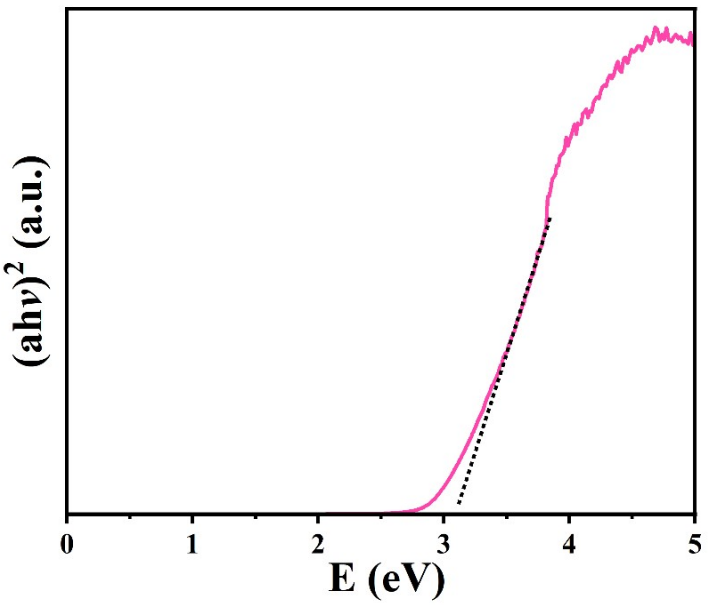

Fig. S22. Tauc plot of the In_2O_3.

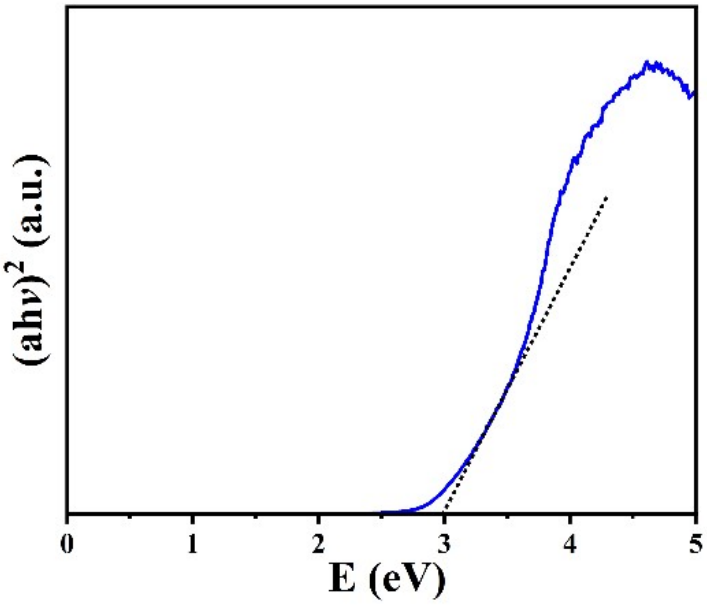

Fig. S23. Tauc plot of the Cu-In_2O_3.

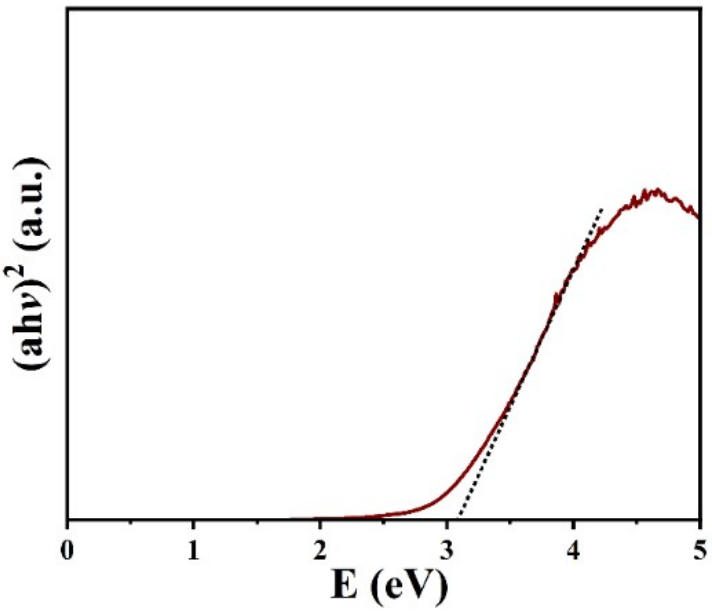

Fig. S24. Tauc plot of the Fe-In_2O_3.

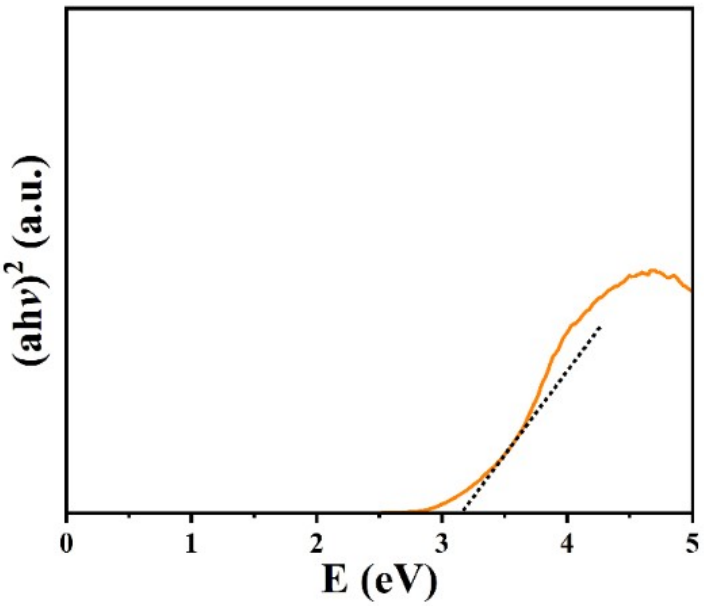

Fig. S25. Tauc plot of the Zn-In_2O_3.

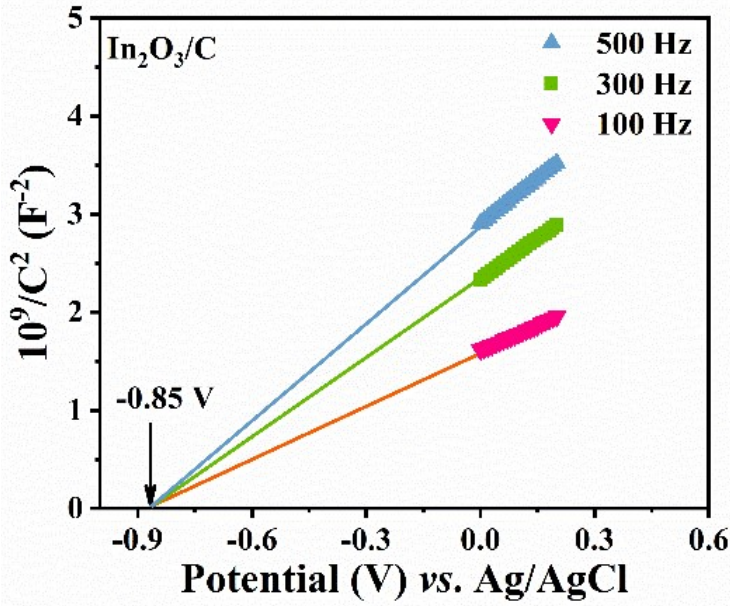

Fig. S26. Mott−Schottky plots of In_2O_3/C.

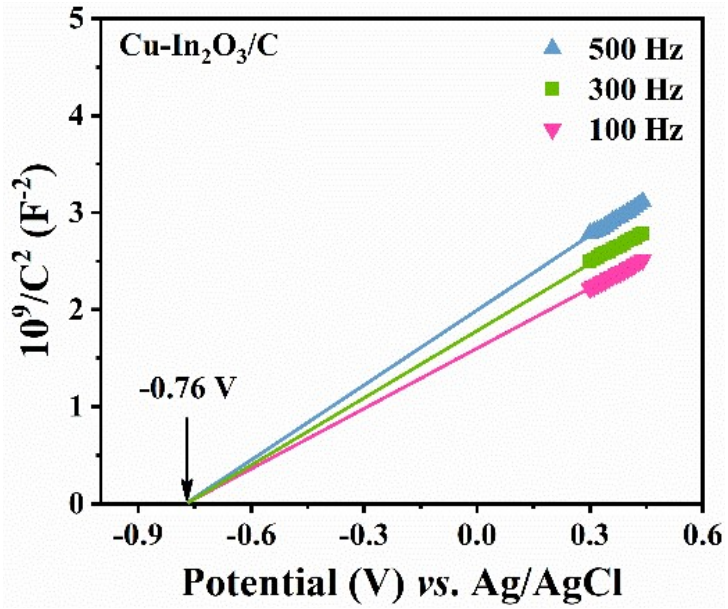

Fig. S27. Mott−Schottky plots of Cu-In_2O_3/C.

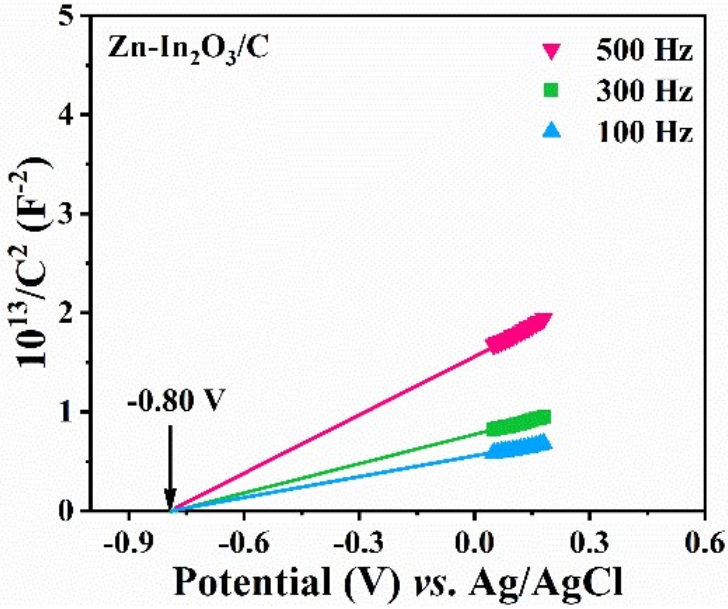

Fig. S28. Mott−Schottky plots of Zn-In_2O_3/C.

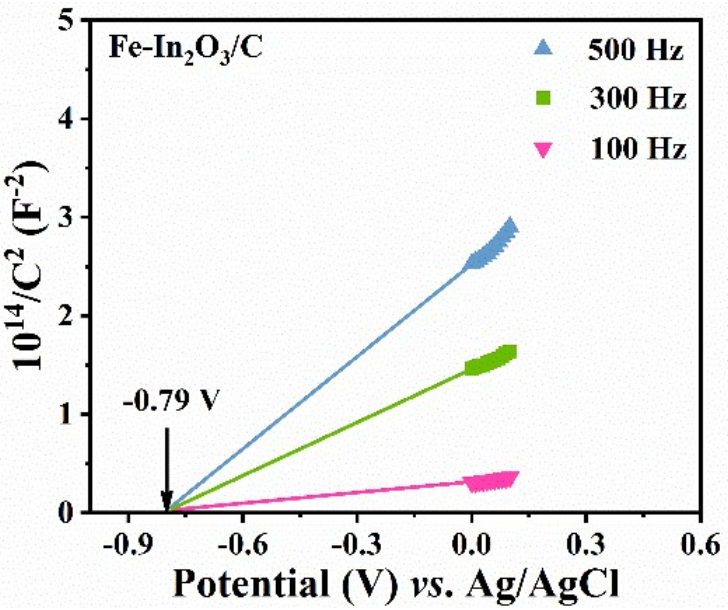

Fig. S29. Mott−Schottky plots of Fe-In_2O_3/C.

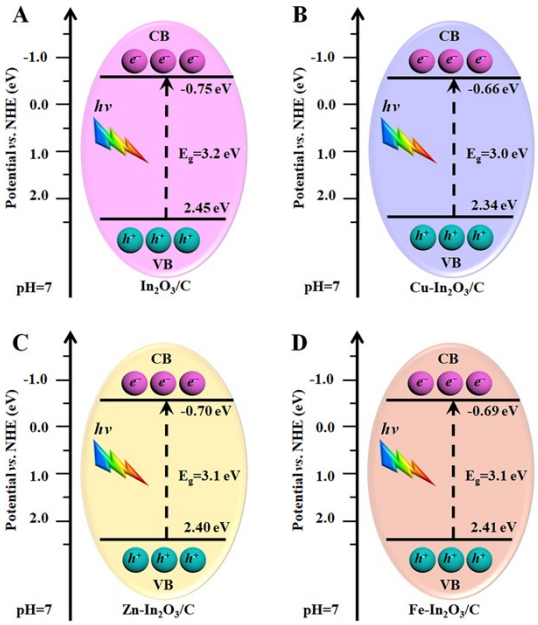

Fig. S30. Schematic illustration of band structure for In_2O_3/C, Cu-In_2O_3/C, Zn-In_2O_3/C, and Fe-In_2O_3/C.

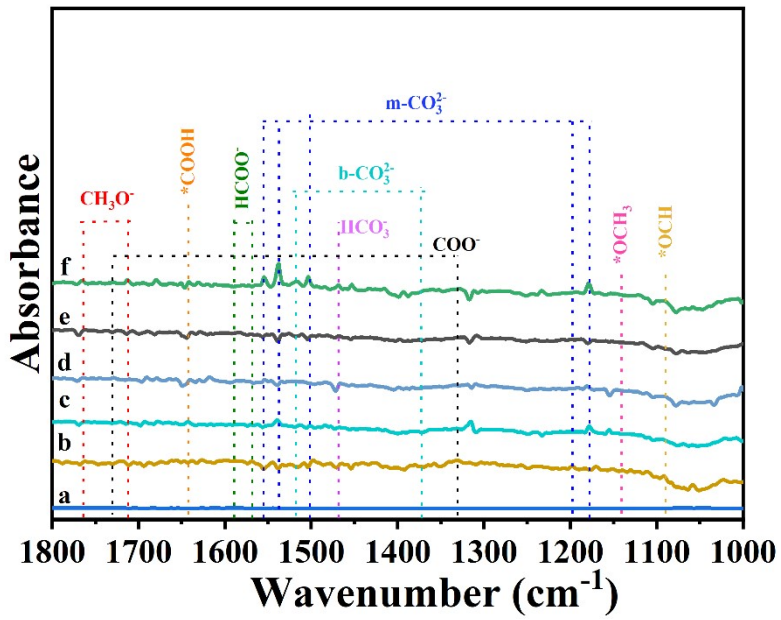

Fig. S31. In-situ DRIFT spectra of In_2O_3/C (a) in darkness, and under visible light irradiation for (b) 5, (c) 10, (d) 15, (e) 20 and (f) 25 min in photocatalytic CO_2 reduction process.

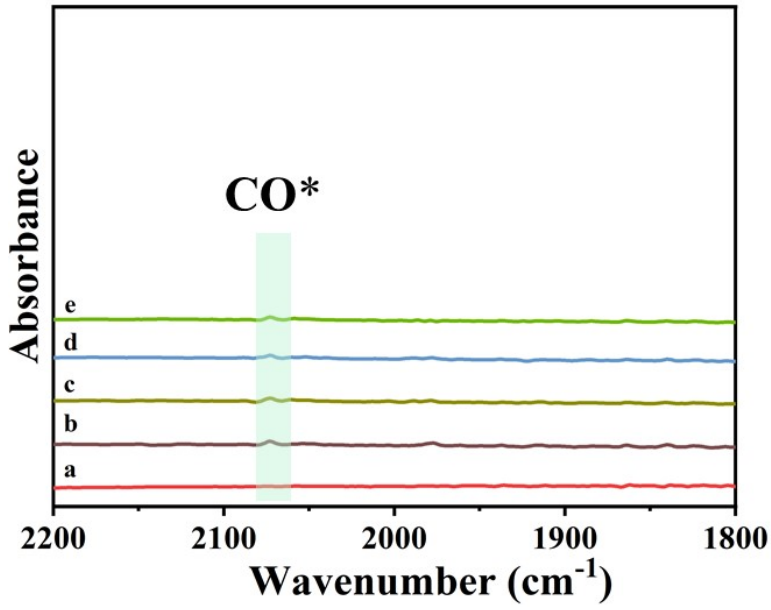

Fig. S32. In-situ DRIFT spectra of Cu-In_2O_3/C (a) in darkness, and under visible light irradiation for (b) 5, (c) 10, (d) 15, (e) 20 and (f) 25 min in photocatalytic CO_2 reduction process.

Table S1. Comparison of previously reported MOF derivatives-based photocatalysts for CO_2 reduction.

Photocatalyst	Illumination range	Photosensitizer	Reaction condition	Product	Production rate (μmol g^{-1} h^{-1})	Selectivity (%)	Ref.
In_2O_3/In_2S_3	>420 nm	/	/	CH_4	14.3	84.7	8
C–In_2O_3@$ZnCo_2O_4$	>320 nm	/	TEA	CO	44.1	66	9
MnS/In_2S_3	Xe lamp	/	TEOA、MeCN	CO	58	/	10
ZnO@Co_3O_4	Xe lamp	/	H_2O	CO	6.51	86.8	11
In_2O_3–CeO_2	Xe lamp	/	/	CO	42.2	77.8	12
Co_3O_4@$CoFe_2O_4$	Xe lamp	$[Ru(bpy)_3]Cl_2$ $6H_2O$	TEOA、H_2O、MeCN	CO	72.2	/	13
$NiCo_2O_4$ HCs	400–800 nm	$[Ru(bpy)_3]Cl_2$ $6H_2O$	TEOA、H_2O、MeCN	CO	10.5	93.4	14
Co_3O_4-NS	400–1000 nm	$[Ru(bpy)_3]Cl_2$ $6H_2O$	TEOA、H_2O、MeCN	CO	4.52	70.1	15
$ZnMn_2O_4$	Xe lamp	/	/	CO	23.99	/	16
CuO_X@p-ZnO	/	/	TEA	CO	27.3	/	17
ZnO/NiO	Xe lamp	/	H_2O	CH_3OH	1.57	/	18
1.0Pt/In_2O_3	500 W Hg lamp	CH_4	H_2O	CH_4	3.54	/	19
Cu-In_2O_3/C	300W Xe lamp	/	H_2O TEA	CO	43.7	78	This work

4. References

1. S. Wang, B. Y. Guan, X. W. D. Lou, *J. Am. Chem. Soc.*, 2018, **140**, 5037.
2. R. Li, L. Sun, W. Zhan, Y.-A. Li, X. Wang, X. Han, *J. Mater. Chem. A*, 2018, **6**, 15747.
3. Q. Liang, X. Yan, Z. Li, Z. Wu, H. Shi, H. Huang and Z. Kang, *J. Mater. Chem. A*, 2022, **10**, 4279.
4. R. Das, K. Das, B. Ray, C. P. Vinod and S. C. Peter, *Energy Environ. Sci.*, 2022, **15**, 1967.
5. K. E. deKrafft, C. Wang, W. Lin, *Adv. Mater.*, 2012, **24**, 2014.
6. C. Zhao, A. Zhou, Y. Dou, J. Zhou, J. Bai, J.-R. Li, *Chem. Eng. J.*, 2021, **416**, 129155.
7. Y. Dou, S.-M. Xu, A. Zhou, H. Wang, J. Zhou, H. Yan, J.-R. Li, *Green Chem. Eng.*, 2020, **1**, 48.
8. D. Yan, Z. Wan, K. Wang, X. Wang, *Chem. Select,* 2021, **6**, 2508.
9. C. Zhao, A. Zhou, Y. Dou, J. Zhou, J. Bai, J.-R. Li, *Chem. Eng. J*. 2021, **416**, 129155.
10. J. Tan, M. Yu, Z. Cai, X. Lou, J. Wang, Z. Li, J. *Colloid. Interface Sci*., 2021, **588**, 547.
11. T. Wang, L. Shi, J. Tang, V. Malgras, S. Asahina, G. Liu, H. Zhang, X. Meng, K. Chang, J. He, O. Terasaki, Y. Yamauchi, J. Ye, *Nanoscale*, 2016, **8**, 6712.
12. Q. Wang, Y. Chen, X. Liu, L. Li, L. Du, G. Tian, *Chem. Eng. J.*, 2021, **421**, 129968.
13. D. Long, X. Li, Z. Yin, S. Fan, P. Wang, *J. Alloy. Compound.,* 2021, **854**, 156942.
14. B. Han, J. Song, S. Liang, W. Chen, H. Deng, X. Ou, Y. -J. Xu, Z. Lin, *Appl. Catal. B Environ*., 2020, **260**, 118208.
15. W. Chen, B. Han, C. Tian, X. Liu, S. Liang, H. Deng, Z. Lin, *Appl. Catal. B Environ*., 2019, **244**, 996.
16. S. Yan, Y. Yu, Y. Cao, *Appl. Surf. Sci.*, 2019, **465**, 383.
17. W. Wang, C. Deng, S. Xie, Y. Li, W. Zhang, H. Sheng, C. Chen, J. Zhao, *J. Am. Chem. Soc.*, 2021, **143**. 2984.
18. S, Chen, J. Yu, J. Zhang, *J. CO_2 Util.*, 2018, **24**, 548.
19. Y.-X. Pan, Y. You, S. Xin, Y. Li, G. Fu, Z. Cui, Y.-L. Men, F.-F. Cao, S.-H. Yu, J. B. Goodenough, *J. Am. Chem. Soc*. 2017, **139**. 4123.